◆ Human Brain Mapping 37:3604–3622 (2016) ◆

Effects of Uncertainty in Head Tissue Conductivity and Complexity on EEG Forward Modeling in Neonates

Hamed Azizollahi,[1] Ardalan Aarabi,[1]* and Fabrice Wallois[1,2]

[1]*GRAMFC, Inserm U1105, University Research Center, Department of Medicine, Amiens University Hospital, Amiens, France*
[2]*EFSN Pediatric (Pediatric Nervous System Functional Investigation Unit), Department of Pediatrics, CHU AMIENS-SITE SUD, Amiens, France*

Abstract: In this study, we investigated the impact of uncertainty in head tissue conductivities and inherent geometrical complexities including fontanels in neonates. Based on MR and CT coregistered images, we created a realistic neonatal head model consisting of scalp, skull, fontanels, cerebrospinal fluid (CSF), gray matter (GM), and white matter (WM). Using computer simulations, we investigated the effects of exclusion of CSF and fontanels, discrimination between GM and WM, and uncertainty in conductivity of neonatal head tissues on EEG forward modeling. We found that exclusion of CSF from the head model induced the strongest widespread effect on the EEG forward solution. Discrimination between GM and white matter also induced a strong widespread effect, but which was less intense than that of CSF exclusion. The results also showed that exclusion of the fontanels from the neonatal head model locally affected areas beneath the fontanels, but this effect was much less pronounced than those of exclusion of CSF and GM/WM discrimination. Changes in GM/WM conductivities by 25% with respect to reference values induced considerable effects in EEG forward solution, but this effect was more pronounced for GM conductivity. Similarly, changes in skull conductivity induced effects in the EEG forward modeling in areas covered by the cranial bones. The least intense effect on EEG was caused by changes in conductivity of the fontanels. Our findings clearly emphasize the impact of uncertainty in conductivity and deficiencies in head tissue compartments on modeling research and localization of brain electrical activity in neonates. *Hum Brain Mapp 37:3604–3622, 2016.*

Key words: electroencephalography; forward modeling; head model; fontanels; finite element method; tissue conductivity; neonates

INTRODUCTION

Electroencephalography (EEG) has become a popular modality, especially for the investigation of brain functions and the diagnosis of neurological disorders [Hughes, 1996; Rampil, 1998; Salinsky et al., 1987; Wieser et al., 2006]. The ultimate goal of functional brain imaging using EEG is to localize cerebral sources generating measured EEG signals using volume conductor models. The accuracy of EEG source localization largely depends on the accuracy of the forward model [Akalin Acar and Makeig, 2013], which

Additional Supporting Information may be found in the online version of this article.

*Correspondence to: Ardalan Aarabi, PhD, GRAMFC, Inserm U 1105, University research center (CURS)-University Hospital of Amiens, CHU AMIENS - SITE SUD, avenue Laennec, 80054, Amiens. E-mail: ardalan.aarabi@u-picardie.fr

Received for publication 28 January 2016; Revised 4 May 2016; Accepted 9 May 2016.

DOI: 10.1002/hbm.23263

Published online 30 May 2016 in Wiley Online Library (wileyonlinelibrary.com).

accordingly requires realistic volume conductor models to relate neural sources to EEG measurements.

Realistic head models incorporate the precise anatomical geometry of scalp, skull, CSF, and brain tissues reconstructed by segmentation of individual magnetic resonance (MR) images. The effect of forward model inaccuracies concerning the geometry and conductivity of the various compartments on the precision of EEG source localization methods have been widely investigated in adults [Akalin Acar and Makeig, 2013]. The main sources of inaccuracies in EEG source analysis are exclusion of cerebrospinal fluid (CSF) [Rice et al., 2013; Vorwerk et al., 2014], skull inhomogeneity [Dannhauer et al., 2011; Lanfer et al., 2012; Li et al., 2007; Marin et al., 1998; Montes-Restrepo et al., 2013; Vorwerk et al., 2014], inhomogeneity of brain tissues [Güllmar et al., 2010; Vorwerk et al., 2014], and uncertainty of head tissue conductivity values [Ramon et al., 2004]. In newborn infants, however, few studies have investigated the effect of these deficiencies on the accuracy of EEG forward modeling and source localization [Gargiulo et al., 2015; Lew et al., 2013; Roche-Labarbe et al., 2008] mainly due to the difficulties in creating realistic head models in neonates. Segmentation of brain MR images constitutes the critical step in creating an accurate neonatal head model. Automatic MRI segmentation of the neonatal brain is challenging due to low contrast, low signal-to-noise ratio, and other complexities [Ghadimi et al., 2008; Lew et al., 2013]. Conversely, the neonatal brain undergoes rapid structural changes during the maturation process, especially in the skull including bony structures and deformable fibrous soft tissue, that is, fontanels. During maturation, the fontanels ossify successively, starting from 9 to 10 weeks of fetal life until several months after birth [Adeyemo and Omotade, 1999; Kiesler and Ricer, 2003; Sadler and Langman, 2000]. Few studies have investigated the effect of opening sutures and fontanels on EEG and MEG source analysis [Gargiulo et al., 2015; Lew et al., 2013; Roche-Labarbe et al. 2008]. Roche-Labarbe et al. [2008] modeled the anterior fontanel as a thinner zone in the skull and showed that the presence of fontanels in volume conductor models introduced errors in the localization of cerebral sources. In addition to the effect of fontanels, Lew et al., [2013] also demonstrated that the conductivity difference between the skull and the fontanels could significantly affect the accuracy of the EEG/MEG forward and inverse modeling. However, compared to other deficiencies in the neonatal head models, it has been shown that fontanels have relatively little effect on the accuracy of EEG source analysis [Gargiulo et al., 2015]. In all of the aforementioned studies, MR images were used to create realistic head models, in which the cranial bones and fontanels were manually segmented based on neuroanatomical knowledge. The resulting neonatal head models did not include precise information on neonatal skull geometry, especially concerning the size and exact position of fontanels and did not consider the effects of the temporal fontanels.

In addition to changes in neonatal head geometry, the electrical properties of head tissues also change during growth. Skull conductivity decreases during the ossification process and fontanels are replaced by less conductive bony structures. Brain tissue conductivity also undergoes significant changes during myelination. In neonates, apart from the fact that that the conductivities of brain tissue compartments are unknown, the conductivity contrast between these compartments can also induce significant effects on the accuracy of EEG forward modeling [Despotovic et al., 2013; Lew et al., 2013; Odabaee et al., 2014].

In this study, we conducted a simulation based on the finite element method (FEM) to assess the effects of structural deficiencies in the neonatal head model and inaccuracy in the conductivity of head tissues on EEG forward modeling in neonates. For this purpose, we used coregistered MR and CT images of one neonate to accurately construct a realistic neonatal head model including gray matter (GM), white matter (WM), CSF, skull, fontanels, and scalp. By distributing high density sources in the GM, oriented perpendicular to the cortical surface and using the standard EEG electrode configuration, we investigated the global, regional, and topographical effects of deficiencies and conductivity uncertainty on the accuracy of the EEG forward model.

MATERIAL AND METHODS

CT and MRI Acquisition

To create a realistic neonatal head model, we used MR and CT images of one healthy male neonate of 42 weeks gestational age at the time of the scan, obtained from the Amiens hospital database. The structural 3D volumetric T2-weighted imaging sequence was acquired on a 1.5 Tesla GE MR scanner with the following sequence parameters: TR = 4,500 ms and TE = 149 ms, and a spatial resolution of $1 \times 0.47 \times 0.47$ mm^3. The images were then resliced to $0.94 \times 0.94 \times 0.94$ mm^3. MR images were then used to extract soft tissues including scalp, GM, and WM as well as CSF. In a separate recording session, the neonate's CT images were recorded using a LightSpeed 16, GE medical system with a spatial resolution of $0.35 \times 0.35 \times 0.63$ mm^3. The CT images were used to extract hard tissues, including skull. As part of routine clinical diagnosis, the CT and MR images were visually inspected by a pediatric neuroradiologist, who reported the neonate's brain to be clinically normal with no discernible lesions or structural deformities. This study was approved by the ethics committee (Commission d'Evaluation Ethique de Recherches NonInterventionelles, CEERNI Avis n° 66). Written consent approved by the ethics committee was obtained from the child's parents.

Coregistration and Segmentation

To create a realistic head model, the MR and CT images were coregistered by interactive clipping of unwanted

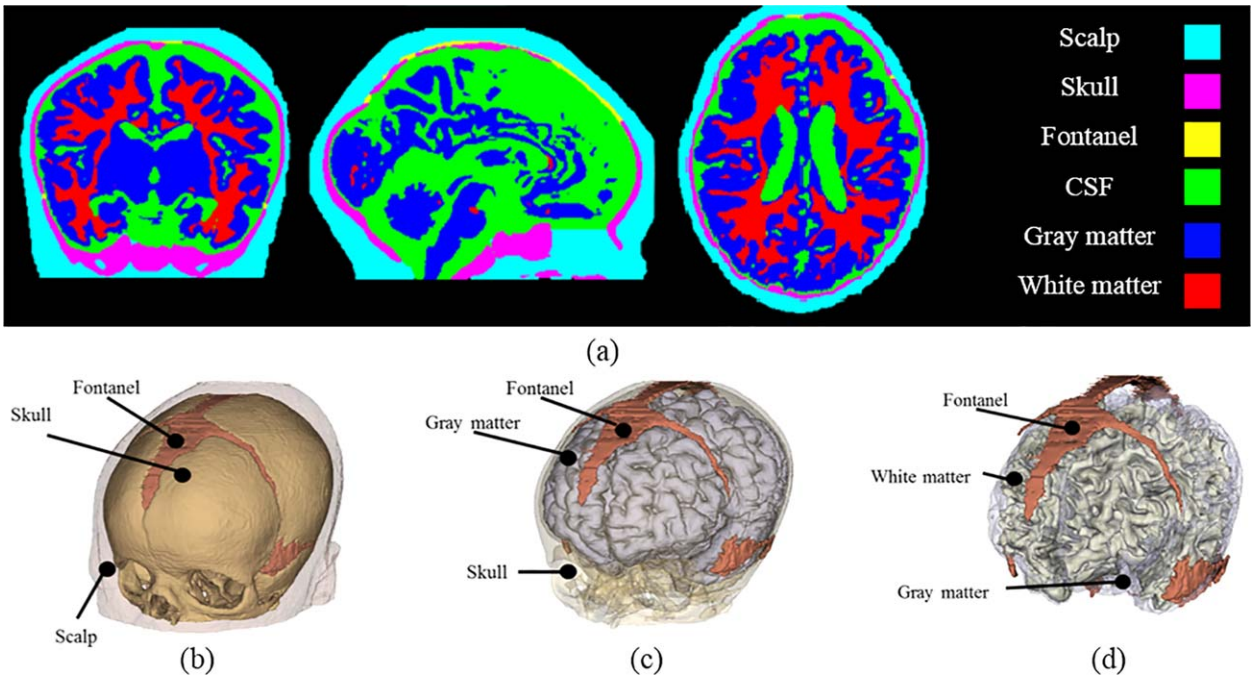

Figure 1.
Coronal, sagittal, and axial planes of the segmented head including GM,WM, CSF, cranial bones, fontanels, and scalp (**a**), and their corresponding 3D reconstruction (**b**). [Color figure can be viewed in the online issue, which is available at wileyonlinelibrary.com.]

parts of the side of the head and the neck. The CT and MR images were then coregistered in SPM8 (Wellcome Trust Centre for Neuroimaging, UCL, London) using the method described by Rorden et al., [2012]. A semi-automatic approach was used to segment the coregistered images, in which GM, WM, and CSF were first segmented using the atlas-segmentation procedure in SPM8 and the probabilistic atlas for full-term neonates [Prastawa et al., 2005]. The cranial bones were then extracted from the CT images using a simple thresholding method and morphological operations were used to fill holes and remove the surplus areas. The fontanels and sutures were manually delineated as gaps between the cranial bones using MRIcro (http://www.mccauslandcenter.sc.edu/mricro/) with the same thickness as their surrounding skull bony structures. The various segmented compartments were then removed from the MR image to obtain the scalp. Automatic and manual corrections were subsequently applied to the segmented compartments to reduce segmentation errors. Figure 1 shows the segmented head compartments and their 3D reconstruction.

Head Model Generation

To create FEM volume conductor head models, the Iso2-mesh toolbox [Fang and Boas, 2009] was applied to the segmented head compartments to construct 1.1 mm resolution tetrahedral meshes containing 633,728 nodes and 3,601,917 FEM elements. In the tetrahedral meshes, FEM elements were labeled as scalp, skull, fontanel, CSF, GM, or WM based on segmentation.

To investigate the effects of head model inaccuracies and conductivity mismatch on EEG forward modeling in neonates, 12 FEM head models were constructed from the generated mesh described above. Test models were created to investigate two different common causes of error in EEG forward modeling in neonates. The first test model set was created to investigate the influence of simplification in the creation of the FEM head model by excluding CSF and fontanels and discriminating between GM and WM. For this purpose, the commonly used FEM head model including only three conductive layers, scalp, skull, and brain (MoldeT1) was used to create three models, ModelT2 with CSF, ModelT3 with GM and WM, and finally the reference model, ModelR including all compartments. The influence of conductivity variations mainly caused by fast changes in conductivities of nearby compartments was investigated by creating the second test model set (ModelT4 – ModelT11) by varying the conductivity of the various compartments by 25% compared to their respective reference values derived from the literature [Lew et al., 2013; Ramon et al., 2004], as summarized in Table I.

TABLE I. Summary of the test/reference models and the compartment conductivities (in S/m) used in the present study

Compartment	$Model_{T1}$	$Model_{T2}$	$Model_{T3}$	$Model_{R}$	$Model_{T4}$	$Model_{T5}$	$Model_{T6}$	$Model_{T7}$	$Model_{T8}$	$Model_{T9}$	$Model_{T10}$	$Model_{T11}$
WM	—	—	0.14	0.14	0.14	0.14	0.14	0.14	0.17	0.11	0.14	0.14
GM	—	—	0.33	0.33	0.33	0.33	0.41	0.25	0.33	0.33	0.33	0.33
Brain	0.33	0.33	··	··	··	··	··	··	··	··	··	··
CSF	—	1.79	1.79	1.79	1.79	1.79	1.79	1.79	1.79	1.79	1.79	1.79
Skull	0.04	0.04	0.04	··	··	··	··	··	··	··	··	··
Cranial bones	—	—	—	0.04	0.05	0.03	0.04	0.04	0.04	0.04	0.04	0.04
Fontanels	—	—	—	0.43	0.43	0.43	0.43	0.43	0.43	0.43	0.54	0.33
Scalp	0.43	0.43	0.43	0.43	0.43	0.43	0.43	0.43	0.43	0.43	0.43	0.43

Abbreviations: WM, white matter; GM, gray matter; CSF, cerebrospinal fluid.

As listed in Table I, we used a conductivity value of 0.04 S/m for the skull in the reference model. Since in a recent study, higher skull conductivity values (0.06–0.2 S/m) have been suggested in neonates [Odabaee et al., 2014], we used ModelT4 with a skull conductivity of 0.2 S/m to further investigate the effect of skull conductivity on forward solutions over a wider range.

EEG Electrodes

The standard 64 electrodes distributed on the scalp based on the 10–10 electrode placement system were used for our simulations. The EEG electrodes were aligned to the FEM head models using fiducials.

Finite Element Forward Simulations

The FEM was used to perform simulations on forward modeling using the FEM head models created. This method has been shown to be highly sophisticated, especially to perform simulations with a high degree of accuracy and computational efficiency on FEM head models with inhomogenities and geometrical complexities such as fontanels and sutures [Lew et al., 2013]. The SimBio-Neuro FEM software (https://www.mrt.uni-jena.de/simbio) implemented in the fieldtrip MATLAB toolbox was used to perform forward simulations for various dipole sources. The software uses the St. Venat direct approach for dipole modeling and the Joint Conjugate Gradient method to compute fluxes in finite element head models [Lew et al., 2009; Wolters et al., 2007]. The numerical calculations were performed using the computational resources of the MeCS platform at the University of Picardie Jules Verne, Amiens, France.

Source Space

As the source space, the cortical surface mesh was extracted from the cortical tetrahedral mesh using the Iso2-mesh toolbox. EEG forward simulations were performed by locating dipole sources in the vertices of the cortical surface mesh with cortical surface normal direction, as shown in Figure 2. To estimate the cortical surface normal direction for each source, the normal vector was computed by averaging the normal vectors of the neighboring triangles. The resulting source space consisted of 324,568 sources evenly distributed on the cortical surface normal direction (Fig. 2).

DIFFERENCE ASSESSMENT

To assess differences in the topography and magnitude of scalp potentials calculated for the FEM volume conductor head models, we used the relative difference measure (RDM) and the logarithmic magnitude difference measure (lnMAG) [Meijs et al., 1989; Vorwerk et al., 2014] as follows:

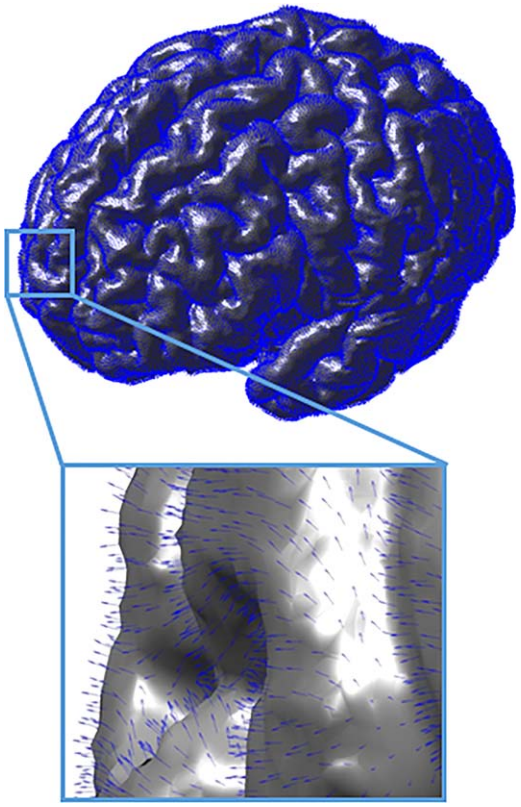

Figure 2.
Distribution of dipolar sources with cortical surface normal direction. [Color figure can be viewed in the online issue, which is available at wileyonlinelibrary.com.]

$$\mathrm{RDM}=\sqrt{\sum_{i=1}^{N}\left(\frac{V_{\mathrm{M2}}}{\sqrt{\sum_{j=1}^{N}V_{\mathrm{M2}}^{2}}}-\frac{V_{\mathrm{M1}}}{\sqrt{\sum_{j=1}^{N}V_{\mathrm{M1}}^{2}}}\right)^{2}} \quad (1)$$

$$\mathrm{lnMAG}=\log\frac{\sqrt{\sum_{j=1}^{N}V_{\mathrm{M1}}^{2}}}{\sqrt{\sum_{j=1}^{N}V_{\mathrm{M2}}^{2}}} \quad (2)$$

where N is the number of EEG electrodes and V_{M1} and V_{M2} denote the computed scalp potentials with Head Model1 and Head Model2, respectively. The RDM shows the topography differences between the forward solutions of the test and reference models. The MAG was defined as the ratio between the overall magnitudes of the test and reference solutions [Vorwerk et al., 2014] over all electrodes. We used a logarithmic scale to better represent differences in signal magnitude (lnMAG) between the test and reference solutions [Vorwerk et al., 2014].

Topographical Maps of RDM and lnMAG

We compared scalp potential topographies computed for the test and reference models to generate the RDM and lnMAG maps to investigate the cortical regions most influenced by differences in structure or conductivity of the compartments under investigation. To more clearly visualize RDM and lnMAG maps in deep sulci, we projected the cortical surface mesh onto the sphere with the conformal mapping [Kwon et al., 2008]. We also used heat maps to clearly visualize the impact of inaccuracies in conductivities and structural deficiencies on scalp potentials computed for the sources located at different distances to the inner skull surface. For this purpose, the distance between the sources and the closest point to the innermost skull layer was calculated. Figure 3 illustrates the distance map between cortical sources and the inner skull layer.

Regional Difference Assessment

To further investigate the impact of various deficiencies or mismatch conductivities on EEG forward modeling, we grouped the EEG electrodes into 13 anatomically different regions (Fig. 4). To identify boundaries between regions, we computed the median of the distances between the position of sources and the electrodes within each group. Each source belonged to the anatomical region presenting the minimum median distance between the source and the region. The advantage of this representation over global representation of the results is that it takes other characteristics of neonatal head geometry, such as spatial symmetry and thickness distribution, into account in interpretation of the results.

RESULTS

The main results of numerical simulations on the global, regional and topographical effects of uncertain head tissue

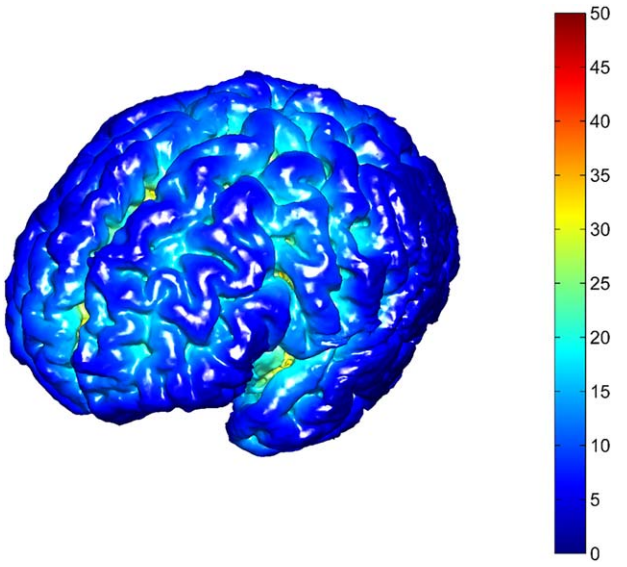

Figure 3.
Distance map computed between cortical sources and the inner skull surface in mm. [Color figure can be viewed in the online issue, which is available at wileyonlinelibrary.com.]

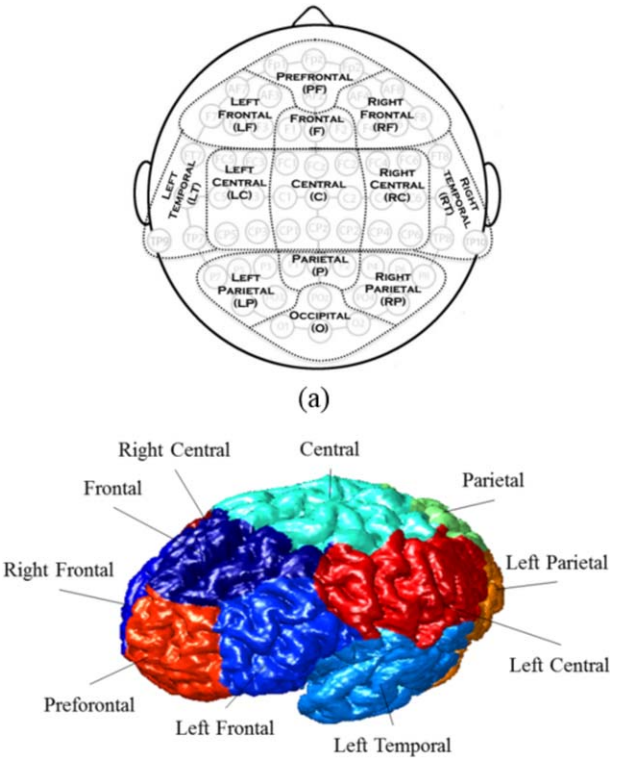

Figure 4.

Montage illustrating the location of 63 electrodes distributed according to the international 10–10 electrode placement system (**a**). The electrodes were grouped according to the thirteen cortical regions of interest (**b**). [Color figure can be viewed in the online issue, which is available at wileyonlinelibrary.com.]

conductivity and structural deficiencies on EEG forward modeling in neonates are presented in the following subsections. The remaining results can be found in Supporting Information.

Global Effect

To demonstrate global effects, we computed the cumulative relative frequencies of RDM and lnMAG, as shown in Figure 5. Exclusion of CSF (ModelT2 vs. ModelT1) and GM/WM discrimination (ModelT3 vs. ModelT2) showed the largest global effects on EEG forward solutions, as depicted in the RDM and lnMAG plots (Fig. 5a,b). GM conductivity (ModelR vs. ModelT6-T7) also showed relatively strong global effects with respect to lnMAG (Fig. 5b). As shown in Figure 5, 25% inaccuracy in fontanel conductivity (ModelR vs. ModelT10-T11) caused the least global effect with respect to both RDM and lnMAG. The effects of exclusion of the fontanels (ModelR vs. ModelT3), changes in skull conductivity (ModelR vs. ModelT4-T5), and variations in WM conductivity (ModelR vs. ModelT8-T9) were also relatively minor as almost 95% of sources fell below 0.1 for RDM and lnMAG (Fig. 5).

Regional Effect

Figure 6 displays the boxplots of the RDM and lnMAG distribution for each of the thirteen brain regions of interest designated in Figure 3. Of all of the various head model deficiencies, exclusion of CSF caused the most widespread effect on forward simulations with RDM and lnMAG varying over the ranges of 0.05 to 0.5 and −0.2 to 1.25, respectively. GM/WM discrimination also showed

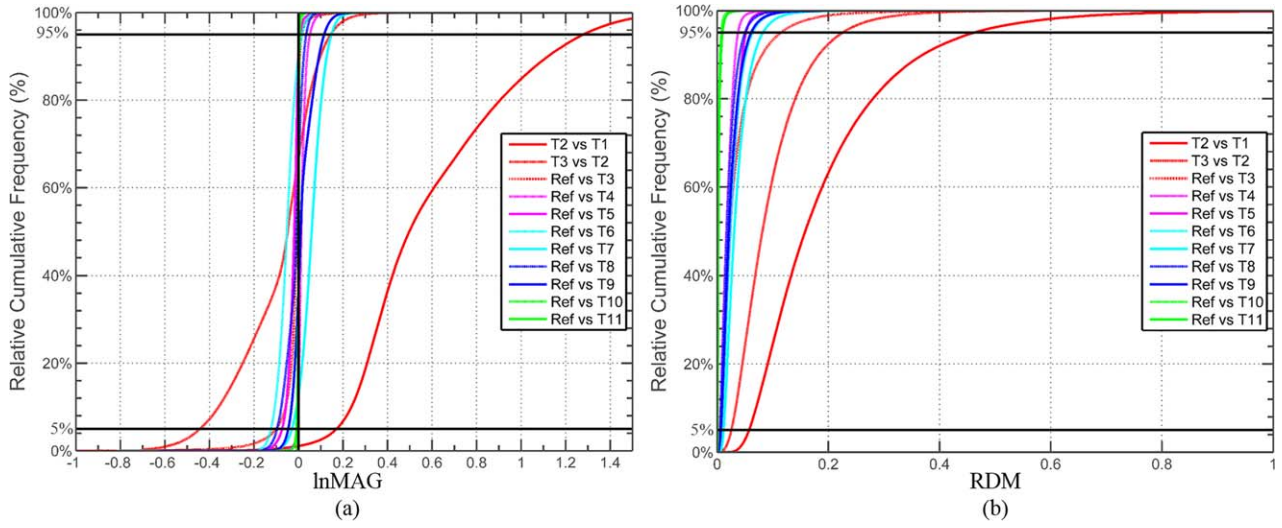

Figure 5.

Cumulative relative frequencies for lnMAG (**a**) and RDM (**b**). The horizontal lines indicate frequencies of 95%.

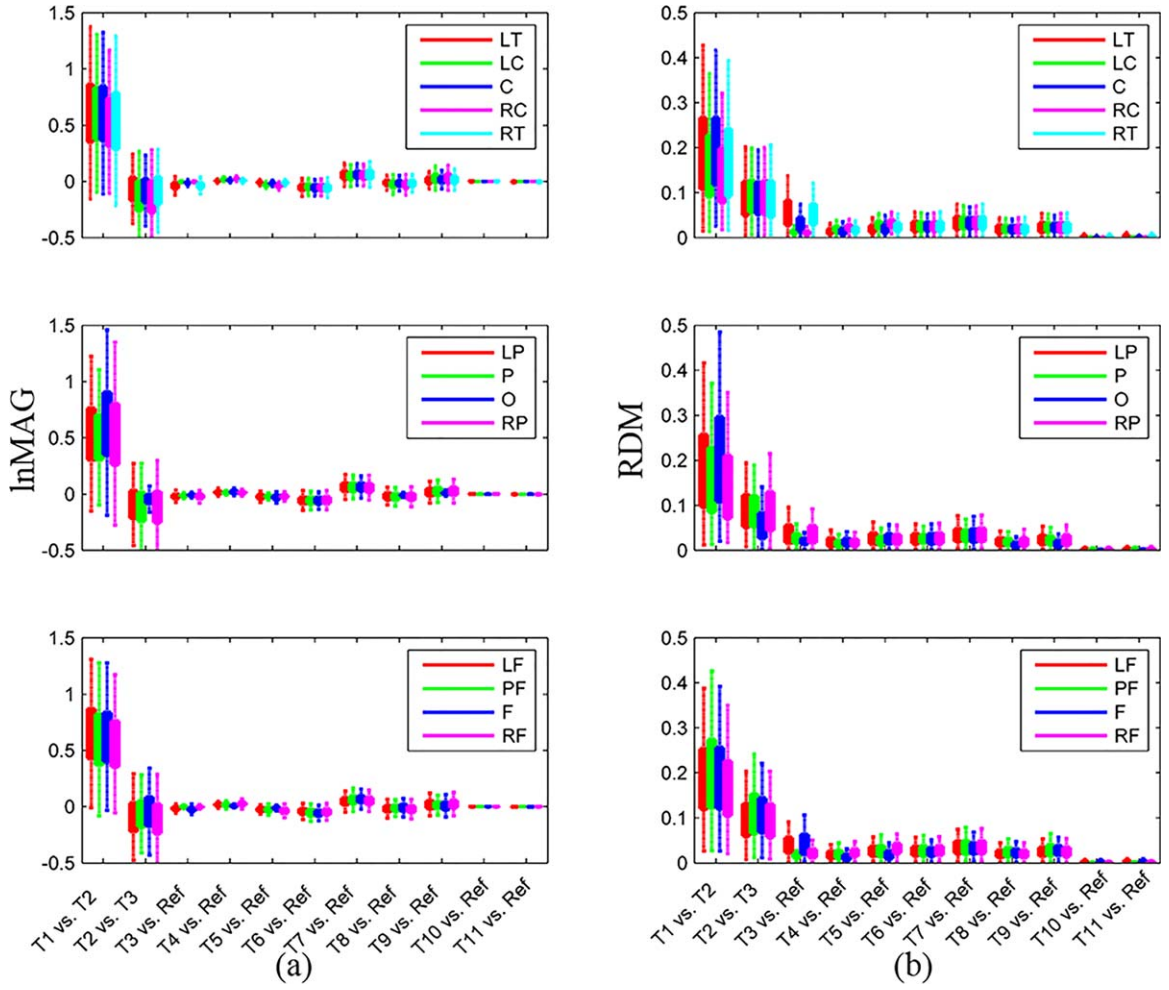

Figure 6.

RDM and lnMAG boxplots reflecting regional effects of inaccuracies in conductivities of the various head compartments and the effects of head model structural deficiencies on EEG forward modeling. See Figure 3 and Table I for abbreviations. [Color figure can be viewed in the online issue, which is available at wileyonlinelibrary.com.]

considerable widespread effects with regard to both RDM (up to 0.25) and lnMAG (−0.5 to 0.45) over all cortical regions except for the occipital lobe. Exclusion of the fontanels and sutures only affected the areas beneath the fontanels in the frontal, bilateral parietal, central and bilateral temporal regions, with a much less intense effect compared to CSF exclusion and GM/WM discrimination. Conversely, variations in skull conductivity influenced scalp potential distributions in the areas covered by cranial bones in the right/left central, occipital and, to a lesser extent, in the right/left frontal regions. As expected, the decrease in skull conductivity leading to increased lnMAG and RDM values resulted from the increased contrast between fontanel and cranial bone conductivity. Changes in GM and WM conductivity values had a limited effect on forward simulations over all cortical regions up to 0.08 for RDM and between −0.15 and 0.07 for lnMAG. As shown in Figure 6, changes in fontanel conductivity by ±25% with respect to reference values resulted in very low RDM and lnMAG values limited to the areas beneath the fontanels.

CSF Exclusion

Figure 7 shows the RDM and lnMAG cortical and spherical maps calculated for ModelT1 compared to ModelT2, reflecting the effect of CSF exclusion on scalp potentials. As shown in Figure 7, the RDM and MAG distribution maps show an intense widespread effect over all cortical areas. Visual inspection of the lnMAG and RDM maps and heat maps (Fig. 8) shows that CSF exclusion had a greater effect on EEG forward solutions for superficial

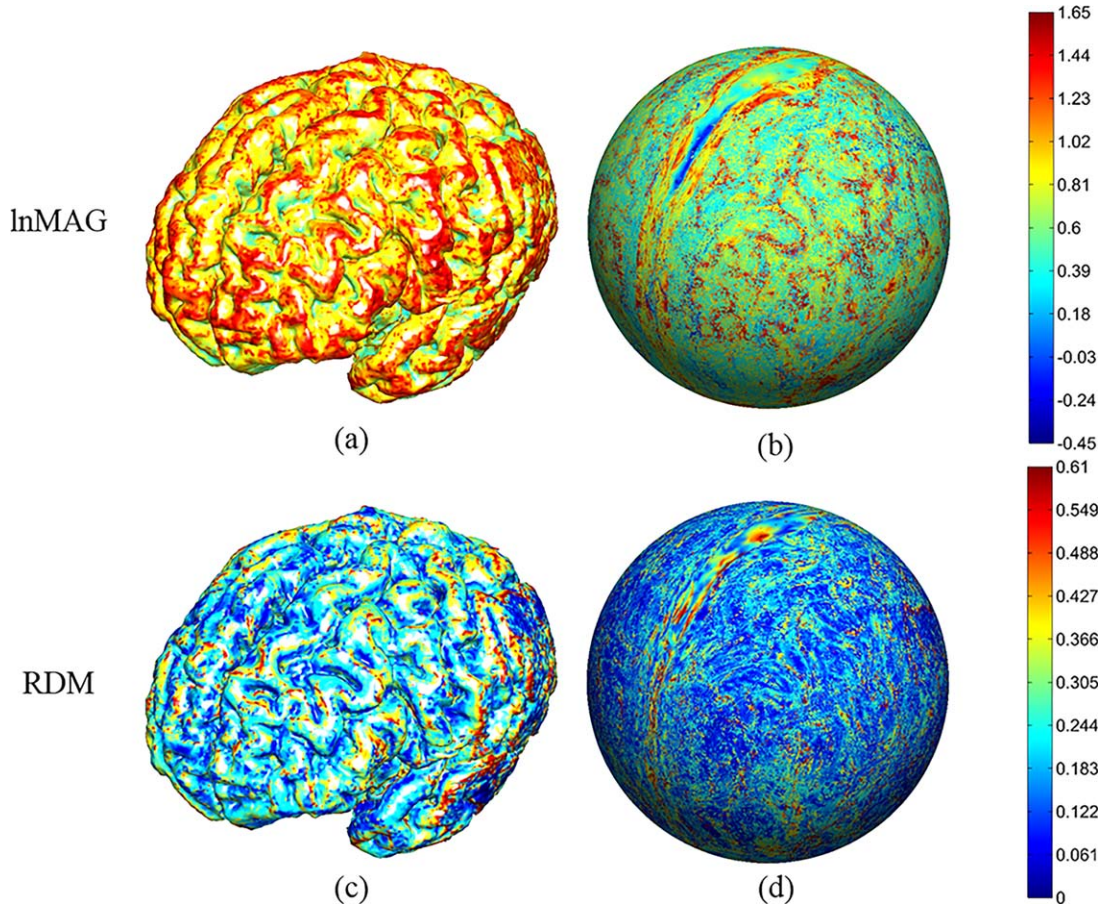

Figure 7.

Effect of CSF exclusion. lnMAG (upper row) and RDM (lower row) cortical (left column) and spherical (right column) maps. RDM and lnMAG were computed between ModelT1 (brain, skull, and scalp, σbrain = 0.33 S/m, σskull = 0.04 S/m, σscalp = 0.43 S/m) and ModelT2 (brain, CSF, skull, and scalp, σbrain = 0.33 S/m, σCSF = 1.79 S/m, σskull = 0.04 S/m, σscalp = 0.43 S/m). The difference between the two models is highlighted in bold. [Color figure can be viewed in the online issue, which is available at wileyonlinelibrary.com.]

sources than for those located in deeper structures. However, a marked effect was nevertheless observed on deeper sources, as RDM and lnMAG (Fig. 8) remained in the ranges of 0.05–0.15 and 0.2–0.4, respectively.

Effect of GM and WM Discrimination

Figure 9 (cortical and spherical maps) and Figure 10 (heat map) show the RDM and lnMAG spatial distribution reflecting the effect of GM and WM discrimination on forward modeling. Although widely affecting all cortical regions, the effect of GM/WM discrimination on forward solutions was relatively limited compared to that of CSF exclusion. As shown in Figure 10, the GM/WM discrimination affected deeper sources to a greater extent.

Effect of Exclusion of Fontanels and Sutures

As shown in Figure 11, exclusion of the fontanels resulted in local effects on the scalp potentials of the sources located beneath the sutures and fontanels and the surrounding areas in the bilateral frontal, central, and temporal lobes. Compared to CSF exclusion and GM/WM discrimination, the effect of fontanel exclusion was relatively minor and regional, as the majority of the affected sources were predominantly superficial, as shown in Figure 12.

Effect of Skull Conductivity

Figures 13 and 14 show the effect of variations in skull conductivity on the forward solutions. As shown by the RDM and lnMAG cortical maps (Fig. 13), a 25% increase in skull conductivity caused minor effects (less than 0.05

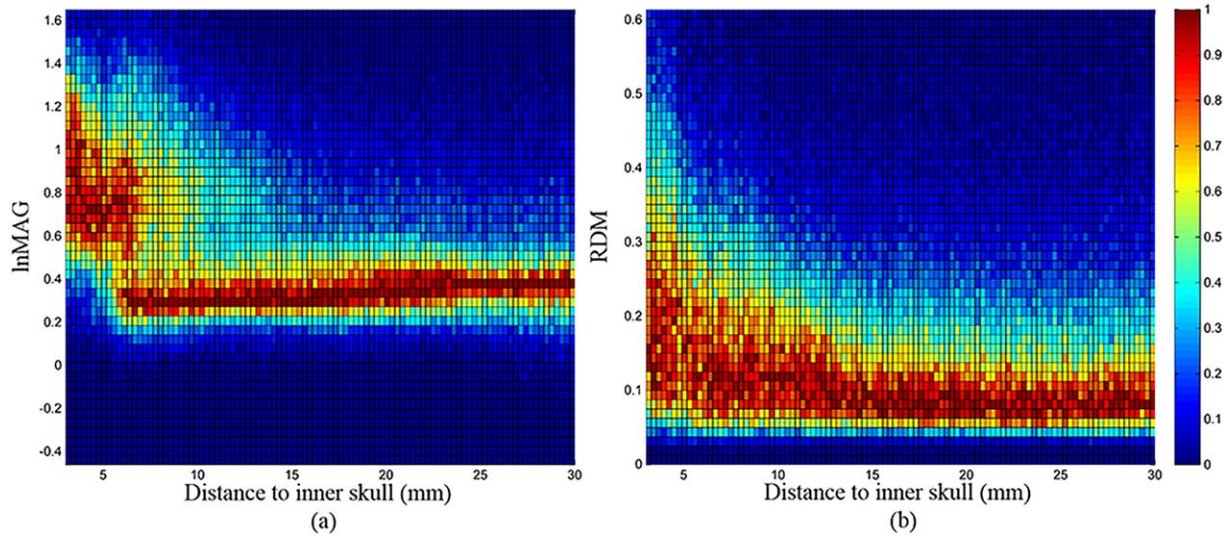

Figure 8.

Effect of CSF exclusion. The 2D heat maps show differences in signal magnitude (lnMAG) and signal topography (RDM) between ModelT1 (brain, skull, and scalp, σbrain = 0.33 S/m, σskull = 0.04 S/m, σscalp = 0.43 S/m) and ModelT2 (brain, CSF, skull, and scalp, σbrain = 0.33 S/m, σCSF = 1.79 S/m, σskull = 0.04 S/m, σscalp = 0.43 S/m). The difference between the two models is highlighted in bold. [Color figure can be viewed in the online issue, which is available at wileyonlinelibrary.com.]

for RDM and between −0.04 and 0.07 for lnMAG) mostly restricted to the sources located in the cortical surface beneath the cranial bones. Furthermore, as shown in Figure 14, the RDM and lnMAG heat maps displayed a descending linear trend from superficial to deep sources. The 25% decrease in skull conductivity also showed a minor local effect with inverted RDM and lnMAG cortical maps (compare Fig. 13 and Supporting Information Fig. S1). As shown in Supporting Information Fig. S3, the increase in skull conductivity up to 0.2 S/m caused proportionally a strong effect on EEG forward solutions with an increase up to 0.3 and 0.38 for RDM and lnMAG, respectively.

Effect of GM and WM Conductivity

Figures 15 and 16, respectively, show the RDM and lnMAG cortical and spherical maps computed by increasing the conductivity of GM and WM by +25% with respect to the values of the reference model. As shown in Figure 15 and Supporting Information Fig. S4, changes in GM conductivity had a considerable effect on the forward solutions. Variations in WM conductivity by ±25% in comparison to the reference model resulted in spatial patterns on the RDM and lnMAG maps (Fig. 16 and Supporting Information Fig. S5) similar to those obtained by GM/WM discrimination (Fig. 9). The heat maps (Fig. 17 and Supporting Information Fig. S6) show imperceptible differences between deep and superficial sources with respect to both RDM and lnMAG. However, compared to the effect of variations in GM and WM conductivities (Figs. 15 and 16), the magnitudes of potential differences due to GM/WM discrimination were more pronounced as shown in Figure 9.

Effect of Fontanel Conductivity

Figure 18 depicts the RDM and lnMAG cortical maps computed by increasing the fontanel conductivity by +25% with respect to the reference values. As for exclusion of the fontanels, changes in fontanel conductivity had only a limited effect (<0.01 for RDM and between −0.01 and 0.01 for lnMAG) restricted to the superficial and deep sources located beneath the fontanels (Figs. 18 and 19). Similar results were obtained by decreasing the fontanel conductivity by 25% with respect to the reference value (Supporting Information Fig. S7 and Fig. S8).

DISCUSSION

To the best of our knowledge, this is the first study to systematically investigate the effect of structural deficiencies and uncertainty in conductivities of head tissue compartments on EEG forward modeling in neonates. Our results show that CSF exclusion and discrimination between GM and WM induced widespread intense effects on the EEG signal with respect to both RDM and lnMAG. However, exclusion of the fontanels and sutures had a local effect on EEG forward solutions in the brain areas located beneath the fontanels. Similarly, changes in skull conductivity resulted in local effects on the scalp potentials

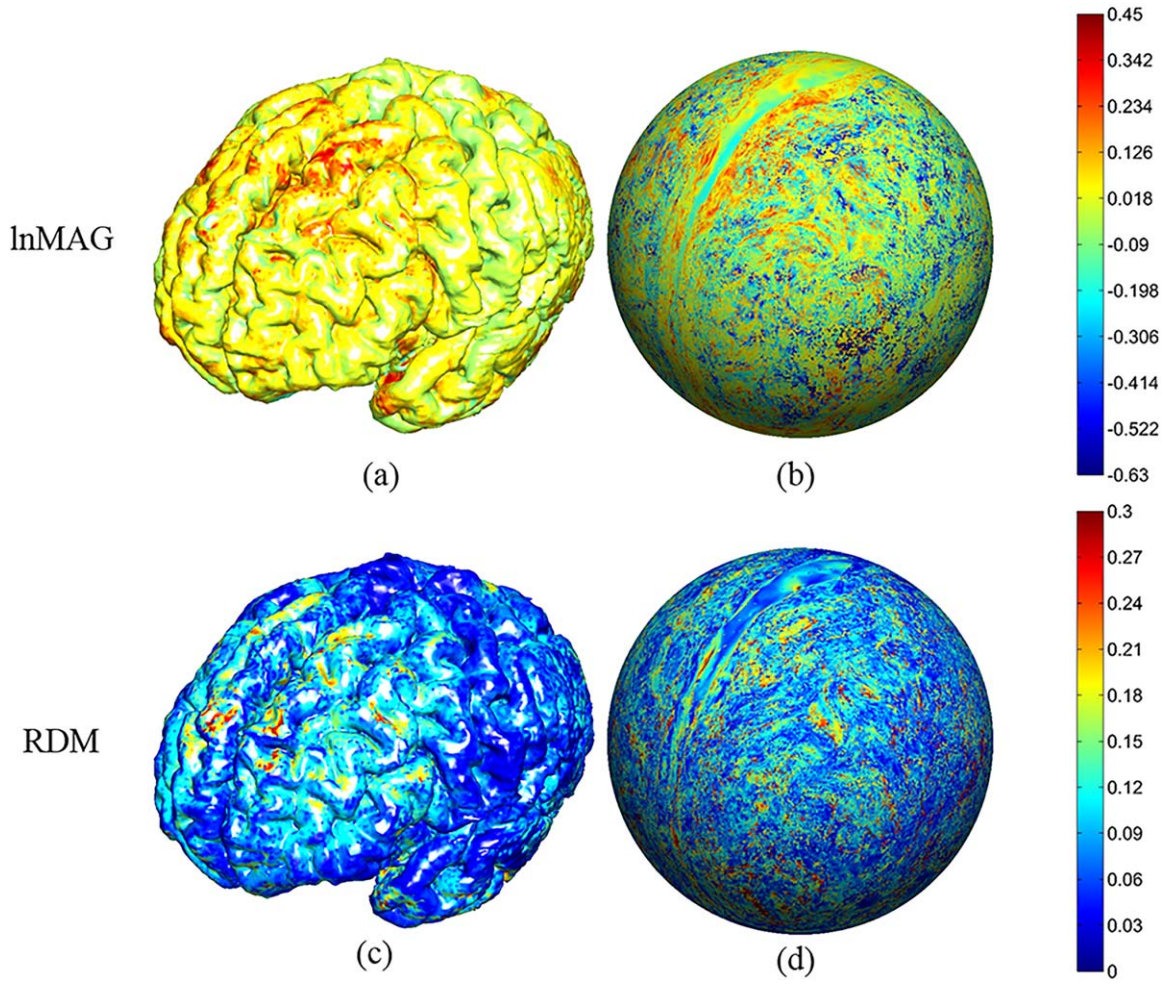

Figure 9.

Effect of gray/white matter discrimination. lnMAG (upper row) and RDM (lower row) cortical (left column) and spherical (right column) maps. RDM and lnMAG were computed between ModelT2 (brain, CSF, skull, and scalp, σbrain = 0.33 S/m, σCSF = 1.79 S/m, σskull = 0.04 S/m, σscalp = 0.43 S/m) and ModelT3 (white matter, gray matter, CSF, skull, and scalp, σWM = 0.14 S/m, σGM = 0.33 S/m, σCSF = 1.79 S/m, σskull = 0.04 S/m, σscalp = 0.43 S/m). The differences between the two models are highlighted in bold. [Color figure can be viewed in the online issue, which is available at wileyonlinelibrary.com.]

of the sources located in the areas covered by the cranial bones. Changes in the GM and WM conductivities also caused considerable effects on the EEG forward simulation, although variations in the WM conductivity caused a weaker effect. Finally, 25% uncertainty in the conductivity of fontanels and sutures with respect to the reference values induced the weakest effect on EEG magnitude and topography.

Effect of CSF

Our results showed the CSF layer had an intense, widespread effect on EEG forward modeling. However, it had a more pronounced effect on EEG signal magnitude (lnMAG) compared to EEG topography (RDM). In line with the findings of previous studies [Ramon et al., 2004; Rice et al., 2013; Vallaghe and Clerc, 2009; Vorwerk et al., 2014], we found that inclusion of CSF in the forward model reduced the EEG scalp potential amplitudes generated by cortical sources especially superficial sources. The effect of CSF on EEG forward modeling has been suggested to be a shunting effect caused by abrupt changes in the conductivity values between brain and skull/scalp layers [Vorwerk et al., 2014]. We found that the shunting effect was slightly more pronounced in frontal and central lobes (Fig. 6). This could be explained by the relationship between the magnitude of the shunting effect and CSF thickness, as increased (or decreased) CSF thickness in any

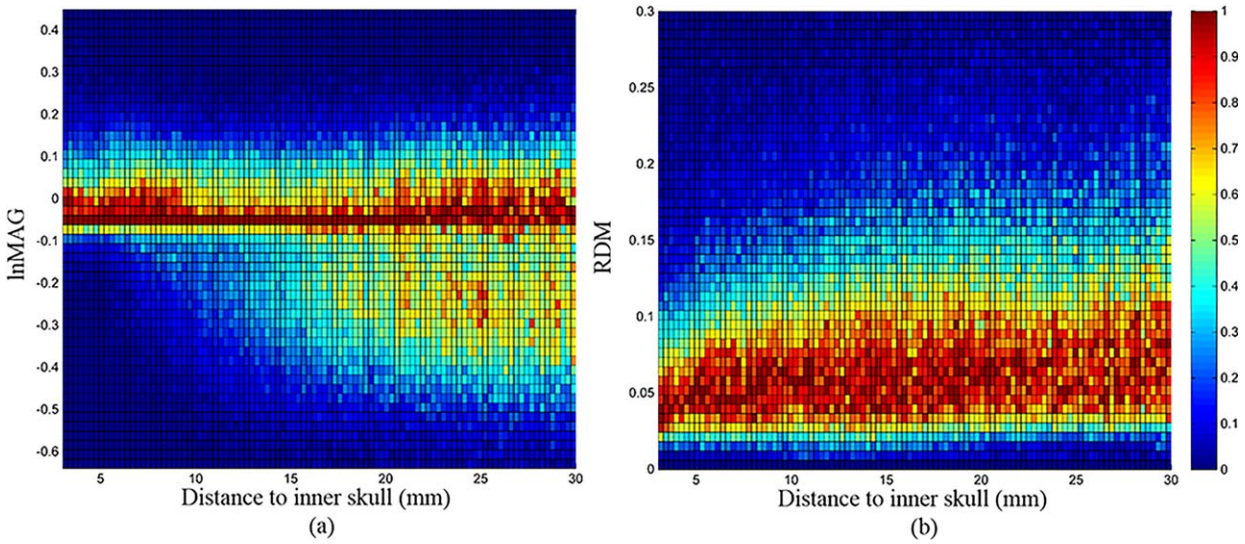

Figure 10.

Effect of gray/white matter discrimination. The 2D heat maps show differences in signal magnitude (lnMAG) and signal topography (RDM) between ModelT2 (brain, CSF, skull, and scalp, σbrain = 0.33 S/m, σCSF = 1.79 S/m, σskull = 0.04 S/m, σscalp = 0.43 S/m) and ModelT3 (white matter, gray matter, CSF, skull, and scalp, σWM = 0.14 S/m, σGM = 0.33 S/m, σCSF = 1.79 S/m, σskull = 0.04 S/m, σscalp = 0.43 S/m). The differences between the two models are highlighted in bold. [Color figure can be viewed in the online issue, which is available at wileyonlinelibrary.com.]

region of interest resulted in decreased (increased) EEG amplitude over that region. This finding is in agreement with the experimental results reported by Rice et al. [2013]. In full-term newborns, CSF thickness has been shown to increase especially at the top of the brain [Beauchamp et al., 2011]. However, changes in CSF thickness can also be related to the position of the neonate's head in the scanner [Wallois et al., 2012]. The shunting effect could therefore change according to the cortical region and the position of the head.

Effect of GM/WM Discrimination

In adults, the discrimination of GM/WM conductivities has been described as a factor largely affecting the results of EEG forward and inverse modeling [Haueisen et al., 2000; Ramon et al., 2004; Vorwerk et al., 2014]. This effect is expected to be more pronounced in neonates, because the conductivity of the brain undergoes changes during the course of neurodevelopment due to the myelination process. Our results show that GM/WM discrimination strongly affected the results of EEG forward modeling. However, in contrast with the effect of CSF inclusion which largely affected superficial sources, the effect of GM/WM discrimination was much more pronounced on deep sources (Figs. 9 and 10). Our results are discordant with those reported by Vorwerk et al. [2014], who showed that CSF inclusion and GM/WM discrimination both strongly affected the EEG topography and magnitude of superficial sources in adults. One possible reason for this discordant result is that, in the study by Vorwerk et al. [2014], the sources were placed on the innermost layer of the GM or, in other words, the outermost layer of the WM. Consequently, the forward solution of the sources is affected by the adjacent contrast in GM/WM conductivity [Haueisen et al., 2000]. This effect can be mathematically described by the surface integral over the WM–GM boundaries [Mosher et al., 1999]. In our study, we located the sources in the outermost layer of the cortical surface, normal to the cortex. This source placement might reduce the effect of GM/WM discrimination, especially for superficial sources. However, deep sources were influenced by this effect to a lesser degree due to the complexity of the brain structure in the sutures. We also found that changes in GM conductivity by $\pm$25% with respect to the reference value had a considerable effect, especially on the EEG magnitude of deep and superficial sources (Figs. 15 and 17). The 25% difference in WM conductivity resulted in changes in EEG amplitude and topography (Fig. 16) similar to, but much less significant than, those observed for the effect of GM/WM discrimination.

Effect of Cranial Bones and Fontanels

The effect of skull deficiencies on EEG forward and inverse modeling in adults has been extensively addressed by many researchers [Ahn et al., 2012; Dannhauer et al., 2011; Li et al., 2007; Lanfer et al., 2012; Marin et al., 1998;

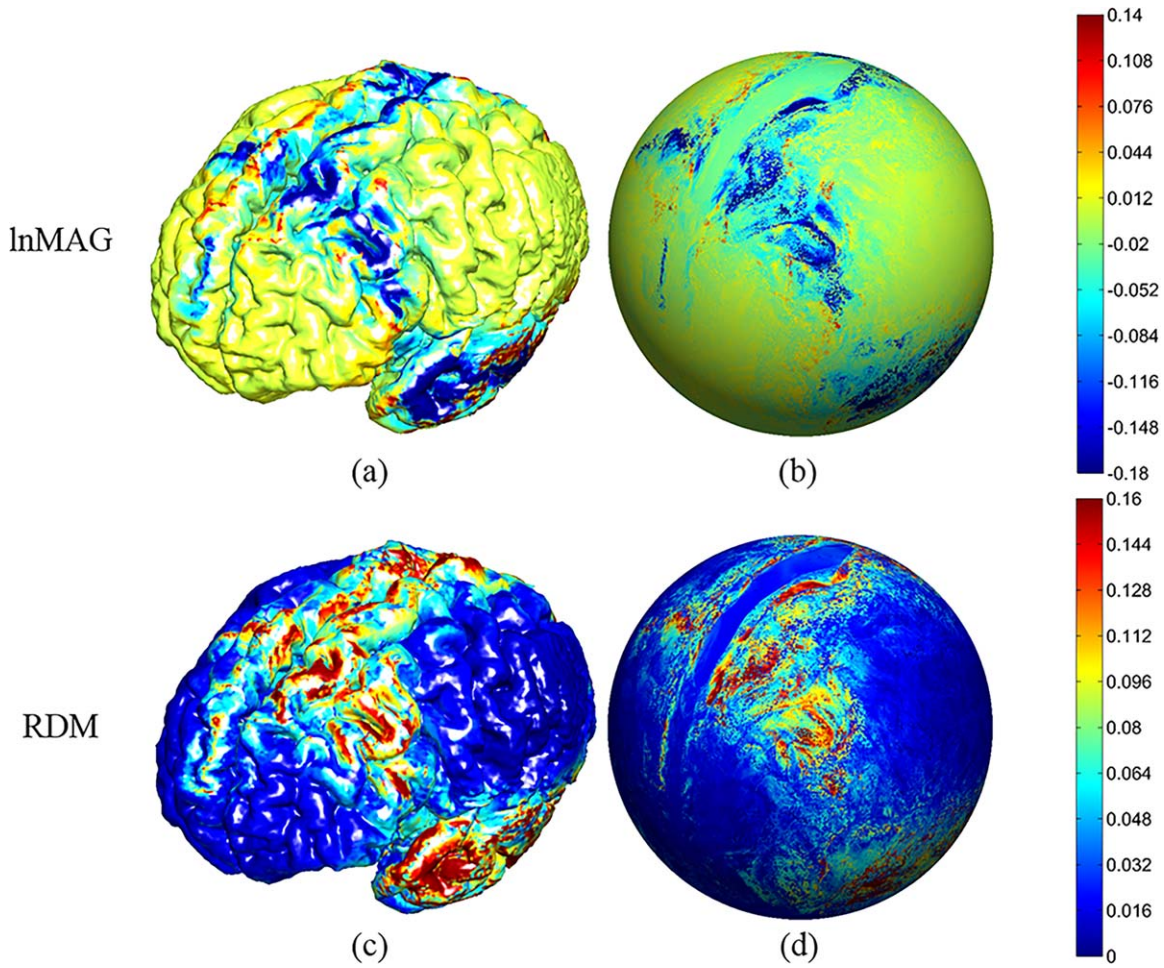

Figure 11.

Effect of exclusion of fontanels and sutures. lnMAG (upper row) and RDM (lower row) cortical (left column) and spherical (right column) maps. RDM and lnMAG were computed between ModelT3 (white matter, gray matter, CSF, skull, and scalp, $\sigma WM = 0.14$ S/m, $\sigma GM = 0.33$ S/m, $\sigma CSF = 1.79$ S/m, $\sigma skull = 0.04$ S/m, $\sigma scalp = 0.43$ S/m) and ModelR (white matter, gray matter, CSF, cranial bones (CB), fontanels, and scalp, $\sigma WM = 0.14$ S/m, $\sigma GM = 0.33$ S/m, $\sigma CSF = 1.79$ S/m, $\sigma CB = 0.04$ S/m, $\sigma fontanel = 0.43$ S/m, $\sigma scalp = 0.43$ S/m). The differences between the two models are highlighted in bold. [Color figure can be viewed in the online issue, which is available at wileyonlinelibrary.com.]

Ramon et al., 2004; Vorwerk et al., 2014]. The neonatal skull presents fundamental structural differences compared to the adult skull. Due to its uncompleted structure, neonatal skull bones are connected by soft and flexible fibrous membranes called fontanels, which are thinner, less ossified and more vascularized than the surrounding bony structures [Roche-Labarbe et al., 2008]. Six fontanels are observed in neonates: anterior and posterior, two mastoid, and two sphenoid [Adeyemo and Omotade, 1999; Kiesler and Ricer, 2003]. The impact of considering the fontanels, especially the anterior fontanel, on both forward and inverse modeling has been investigated in a few studies [Gargiulo et al., 2015 ; Lew et al., 2013; Roche-Labarbe et al., 2008]. In these studies, the fontanels were not correctly extracted from the head MR images due to the lack of information concerning the geometrical structure of cranial bones and fontanels on MR images related to the weak MR signal derived from bony structures. In this study, co-registered CT-MR images were used to construct a realistic head model including detailed information on cranial bones and all six fontanels.

Our results show that exclusion of the fontanels and sutures from the head model locally affected the EEG forward solution, especially in the areas located beneath the fontanels (Figs. 6 and 11). However, this effect was much less pronounced than the effects of CSF exclusion and GM/

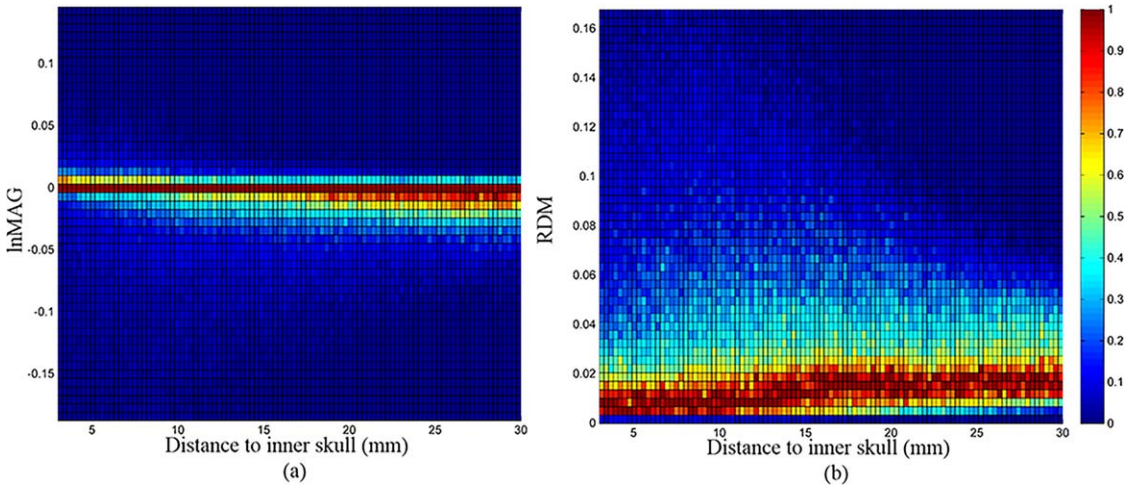

Figure 12.

Effect of exclusion of fontanels and sutures. The 2D heat maps show differences in signal magnitude (lnMAG) and signal topography (RDM) between ModelT3 (white matter, gray matter, CSF, skull, and scalp, $\sigma WM = 0.14$ S/m, $\sigma GM = 0.33$ S/m, $\sigma CSF = 1.79$ S/m, $\sigma skull = 0.04$ S/m, $\sigma scalp = 0.43$ S/m) and ModelR (white matter, gray matter, CSF, cranial bones (CB), fontanels, and scalp, $\sigma WM = 0.14$ S/m, $\sigma GM = 0.33$ S/m, $\sigma CSF = 1.79$ S/m, $\sigma CB = 0.04$ S/m, $\sigma fontanel = 0.43$ S/m, $\sigma scalp = 0.43$ S/m). The differences between the two models are highlighted in bold. [Color figure can be viewed in the online issue, which is available at wileyonlinelibrary.com.]

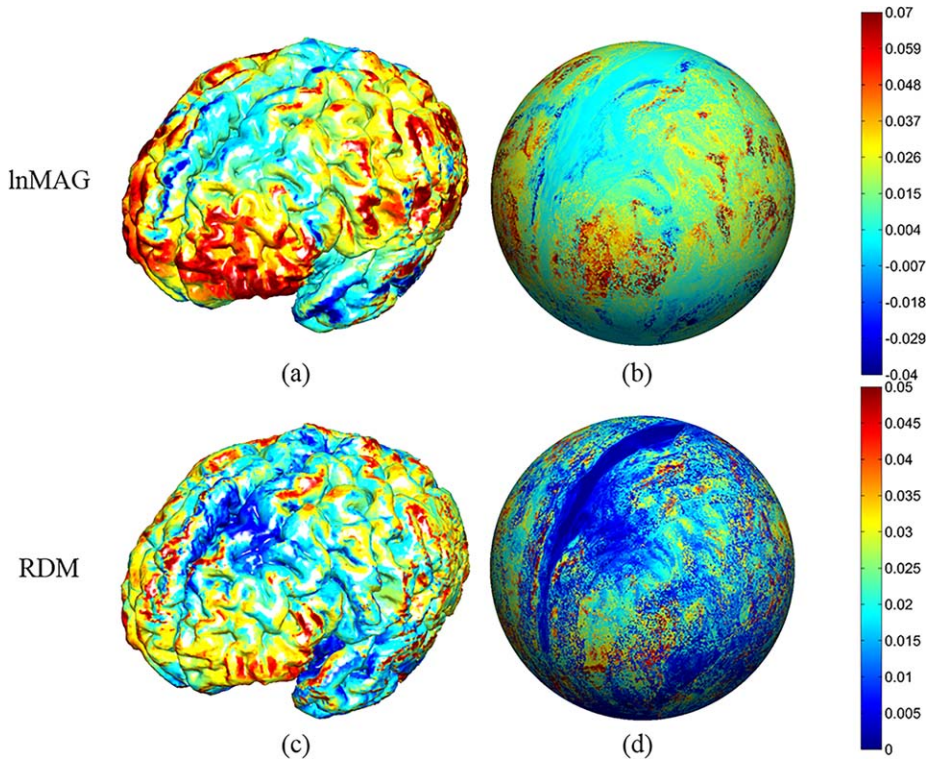

Figure 13.

Effect of skull conductivity. lnMAG (upper row) and RDM (lower row) cortical (left column) and spherical (right column) maps. RDM and lnMAG were computed between ModelT4 (white matter, gray matter, CSF, cranial bones (CB), fontanels, and scalp, $\sigma WM = 0.14$ S/m, $\sigma GM = 0.33$ S/m, $\sigma CSF = 1.79$ S/m, $\sigma CB = 0.05$ S/m, $\sigma fontanel = 0.43$ S/m, $\sigma scalp = 0.43$ S/m) and ModelR (white matter, gray matter, CSF, cranial bones, fontanels, and scalp, $\sigma WM = 0.14$ S/m, $\sigma GM = 0.33$ S/m, $\sigma CSF = 1.79$ S/m, $\sigma CB = 0.04$ S/m, $\sigma fontanel = 0.43$ S/m, $\sigma scalp = 0.43$ S/m). The difference between the two models is highlighted in bold. [Color figure can be viewed in the online issue, which is available at wileyonlinelibrary.com.]

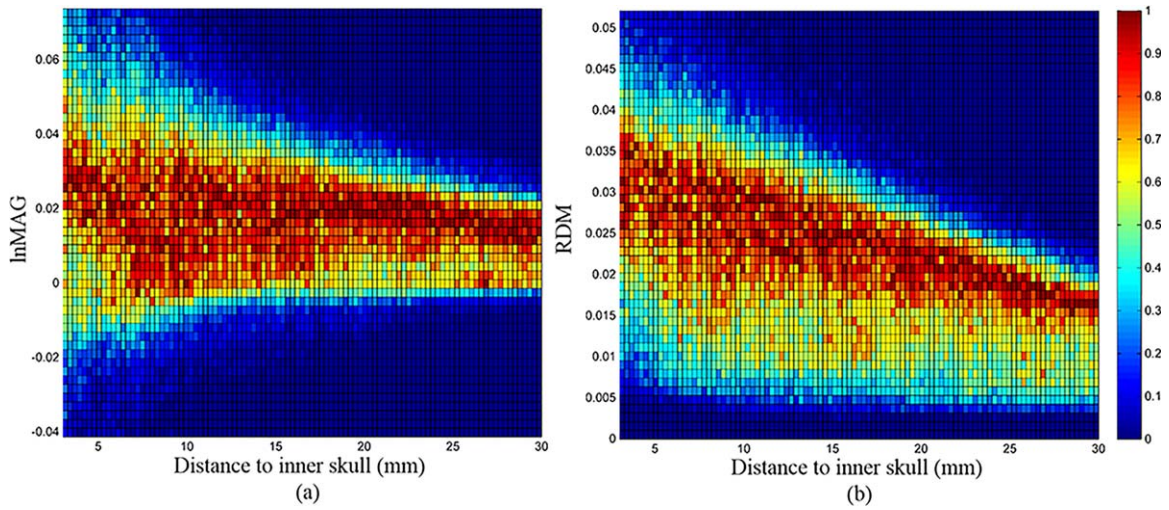

Figure 14.

Effect of skull conductivity. The 2D heat maps show differences in signal magnitude (lnMAG) and signal topography (RDM) between ModelT4 (white matter, gray matter, CSF, cranial bones (CB), fontanels, and scalp, σWM = 0.14 S/m, σGM = 0.33 S/m, σCSF = 1.79 S/m, σCB = 0.05 S/m, σfontanel = 0.43 S/m, σscalp = 0.43 S/m) and ModelR (white matter, gray matter, CSF, cranial bones, fontanels, and scalp, σWM = 0.14 S/m, σGM = 0.33 S/m, σCSF = 1.79 S/m, σCB = 0.04 S/m, σfontanel = 0.43 S/m, σscalp = 0.43 S/m). The difference between the two models is highlighted in bold. [Color figure can be viewed in the online issue, which is available at wileyonlinelibrary.com.]

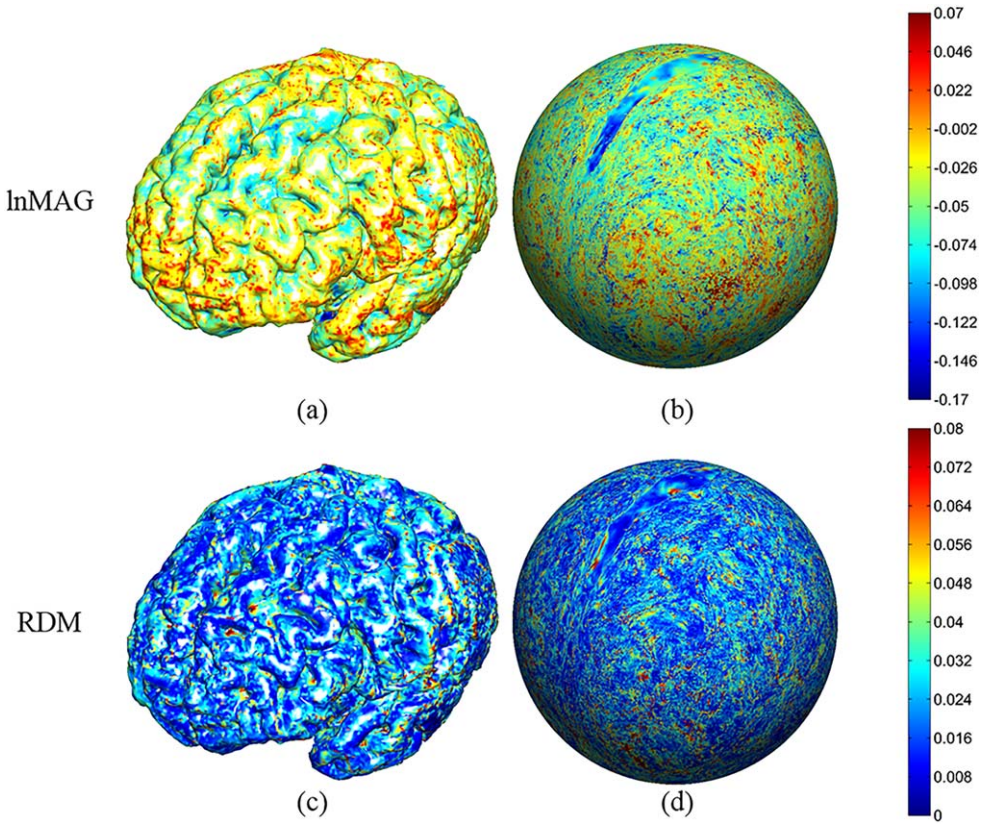

Figure 15.

Effect of gray matter conductivity. lnMAG (upper row) and RDM (lower row) cortical (left column) and spherical (right column) maps. RDM and lnMAG were computed between ModelT6 (white matter, gray matter, CSF, cranial bones (CB), fontanels, and scalp, σWM = 0.14 S/m, σGM = 0.41 S/m, σCSF = 1.79 S/m, σCB = 0.05 S/m, σfontanel = 0.43 S/m, σscalp = 0.43 S/m) and ModelR (white matter, gray matter, CSF, cranial bones, fontanels, and scalp, σWM = 0.14 S/m, σGM = 0.33 S/m, σCSF = 1.79 S/m, σCB = 0.04 S/m, σfontanel = 0.43 S/m, σscalp = 0.43 S/m). The difference between the two models is highlighted in bold. [Color figure can be viewed in the online issue, which is available at wileyonlinelibrary.com.]

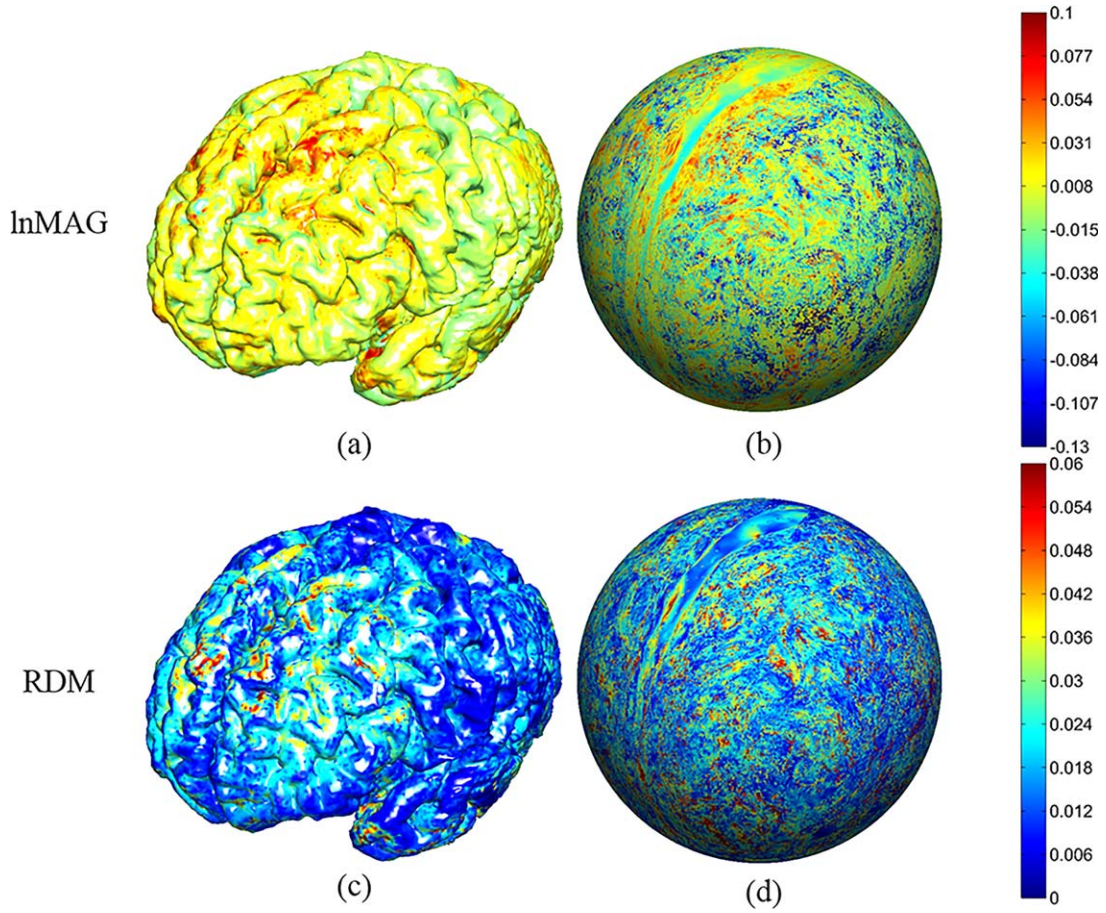

Figure 16.

Effect of white matter conductivity. lnMAG (upper row) and RDM (lower row) cortical (left column) and spherical (right column) maps. RDM and lnMAG were computed between ModelT8 (white matter, gray matter, CSF, cranial bones (CB), fontanels, and scalp, $\sigma WM = 0.17$ S/m, $\sigma GM = 0.33$ S/m, $\sigma CSF = 1.79$ S/m, $\sigma CB = 0.05$ S/m, $\sigma fontanel = 0.43$ S/m, $\sigma scalp = 0.43$ S/m) and ModelR (white matter, gray matter, CSF, cranial bones, fontanels, and scalp, $\sigma WM = 0.14$ S/m, $\sigma GM = 0.33$ S/m, $\sigma CSF = 1.79$ S/m, $\sigma CB = 0.04$ S/m, $\sigma fontanel = 0.43$ S/m, $\sigma scalp = 0.43$ S/m). The difference between the two models is highlighted in bold. [Color figure can be viewed in the online issue, which is available at wileyonlinelibrary.com.]

WM discrimination, suggesting that the fontanels, especially those partly covering the temporal areas, may have only a minor impact on the results of the inverse solution, especially for the sources of the neuronal activity related to language [Mahmoudzadeh et al., 2013; Wallois et al., 2012;].

In addition, human skull conductivity undergoes rapid and dramatic changes during maturation from infancy to adulthood [Lew et al., 2013; Odabaee et al., 2014]. This rapid change can lead to overestimation or underestimation of skull conductivity in neonates. The real value of neonatal skull conductivity has not been precisely determined, but is likely to be more than that estimated for adults. In our study, we used a skull conductivity of 0.04 S/m, which has been measured experimentally in neonatal piglets [Pant et al., 2011]. Our results also show that underestimation/overestimation of skull conductivity by 25% with respect to the reference conductivity value can slightly affect the EEG forward solutions, especially in the areas underneath the cranial bones (e.g., prefrontal, right/left central and occipital). However, in line with previous findings [Gargiulo et al., 2015.; Lew et al., 2013], our results indicated that underestimation of skull conductivity could have more pronounced effects on EEG forward simulation compared to overestimation. This difference could be explained by the decreased contrast between the fontanels and skull conductivity when skull conductivity is underestimated.

In neonates, Odabaee et al. [2014] have suggested higher skull conductivity values (up to 0.2 S/m) for the skull close to that of soft tissues. We performed forward simulations using a skull conductivity of 0.2 S/m. The spatial distributions of RDM and lnMAG as shown in Fig. 13 and

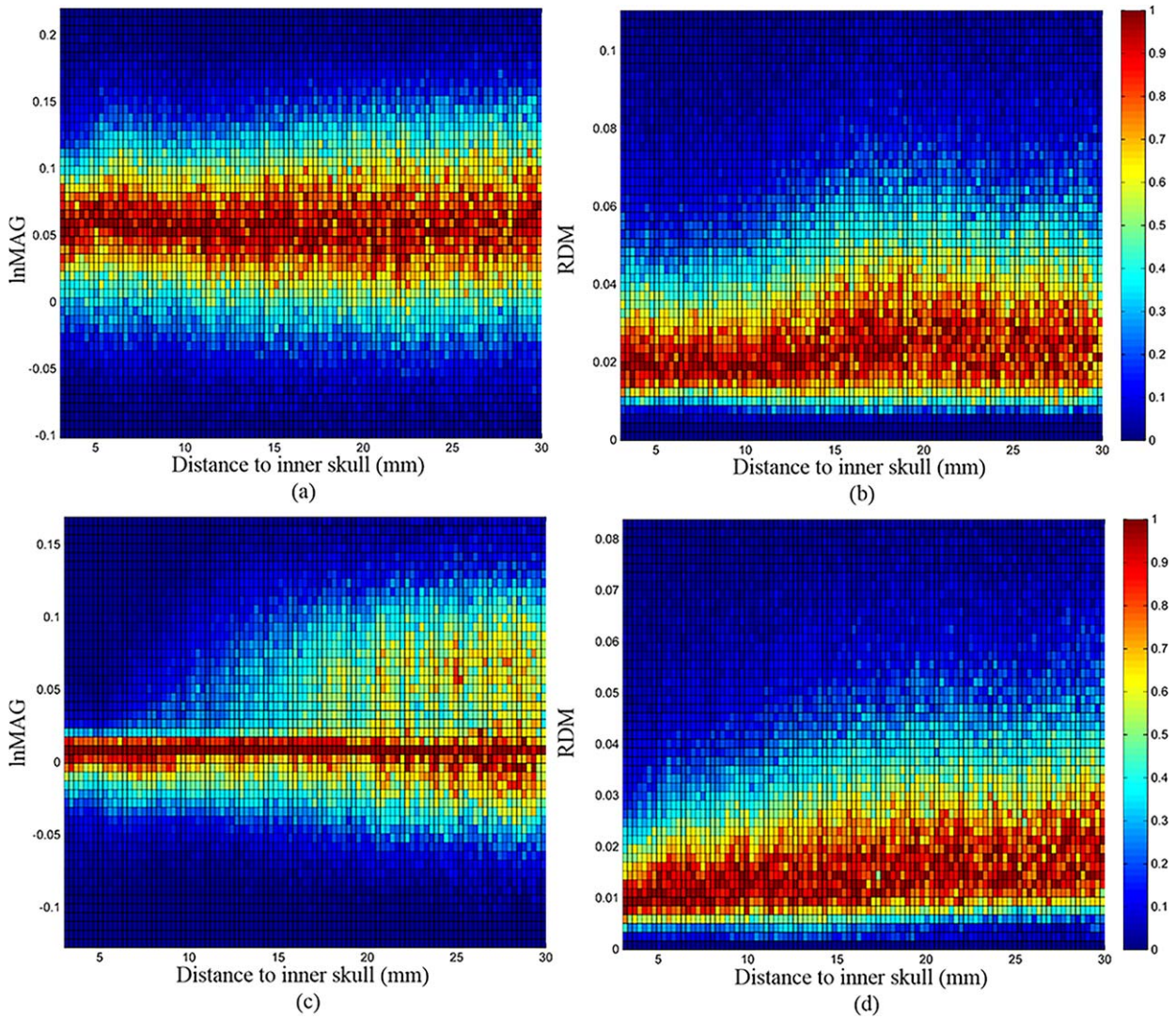

Figure 17.

Effect of gray matter and white matter conductivity. The 2D heat maps show differences in signal magnitude (lnMAG) and signal topography (RDM) between ModelT6 (white matter, gray matter, CSF, cranial bones (CB), fontanels, and scalp, $\sigma WM = 0.14$ S/m, $\sigma GM = 0.41$ S/m, $\sigma CSF = 1.79$ S/m, $\sigma CB = 0.05$ S/m, $\sigma fontanel = 0.43$ S/m, $\sigma scalp = 0.43$ S/m), ModelT8 (white matter, gray matter, CSF, cranial bones (CB), fontanels, and scalp, $\sigma WM = 0.17$ S/m, $\sigma GM = 0.33$ S/m, $\sigma CSF = 1.79$ S/m, $\sigma CB = 0.05$ S/m, $\sigma fontanel = 0.43$ S/m, $\sigma scalp = 0.43$ S/m) and ModelR (white matter, gray matter, CSF, cranial bones, fontanels, and scalp, $\sigma WM = 0.14$ S/m, $\sigma GM = 0.33$ S/m, $\sigma CSF = 1.79$ S/m, $\sigma CB = 0.04$ S/m, $\sigma fontanel = 0.43$ S/m, $\sigma scalp = 0.43$ S/m). The differences between the three models are highlighted in bold. Plots (**a-b**) and (**c-d**) show differences between (ModelT6 and ModelR) and (ModelT8 and ModelR), respectively. [Color figure can be viewed in the online issue, which is available at wileyonlinelibrary.com.]

Supporting Information Fig. S3 were similar for the two conductivity values (0.05 and 0.2 S/m). However, we found that the effect of skull conductivity on EEG forward solutions became more prominent with increasing conductivity.

We also investigated the effect of 25% variations in fontanel conductivity with respect to the reference value on EEG forward modeling. Variation in fontanel conductivity is thought to occur during the ossification process, starting approximately at 11 weeks of gestational age, resulting in a gradual decrease in the conductivity of the fontanels in the course of development. Our results show that changes in fontanel conductivity cause only minor effects on RDM and lnMAG, especially in frontal, central, parietal, and temporal areas located beneath the fontanels.

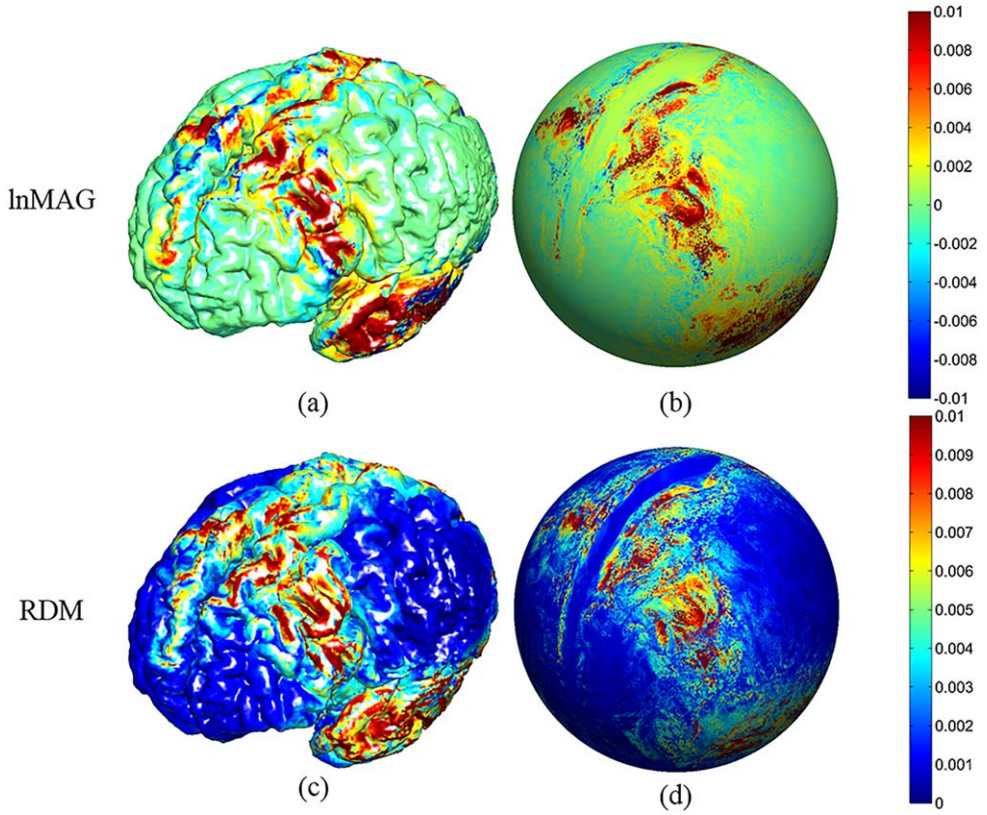

Figure 18.

Effect of fontanel conductivity. lnMAG (upper row) and RDM (lower row) cortical (left column) and spherical (right column) maps. RDM and lnMAG were computed between ModelT10 (white matter, gray matter, CSF, cranial bones (CB), fontanels, and scalp, $\sigma WM = 0.14$ S/m, $\sigma GM = 0.41$ S/m, $\sigma CSF = 1.79$ S/m, $\sigma CB = 0.04$ S/m, $\sigma fontanel = 0.54$ S/m, $\sigma scalp = 0.43$ S/m) and ModelR (white matter, gray matter, CSF, cranial bones, fontanels, and scalp, $\sigma WM = 0.14$ S/m, $\sigma GM = 0.33$ S/m, $\sigma CSF = 1.79$ S/m, $\sigma CB = 0.04$ S/m, $\sigma fontanel = 0.43$ S/m, $\sigma scalp = 0.43$ S/m). The difference between the two models is highlighted in bold. [Color figure can be viewed in the online issue, which is available at wileyonlinelibrary.com.]

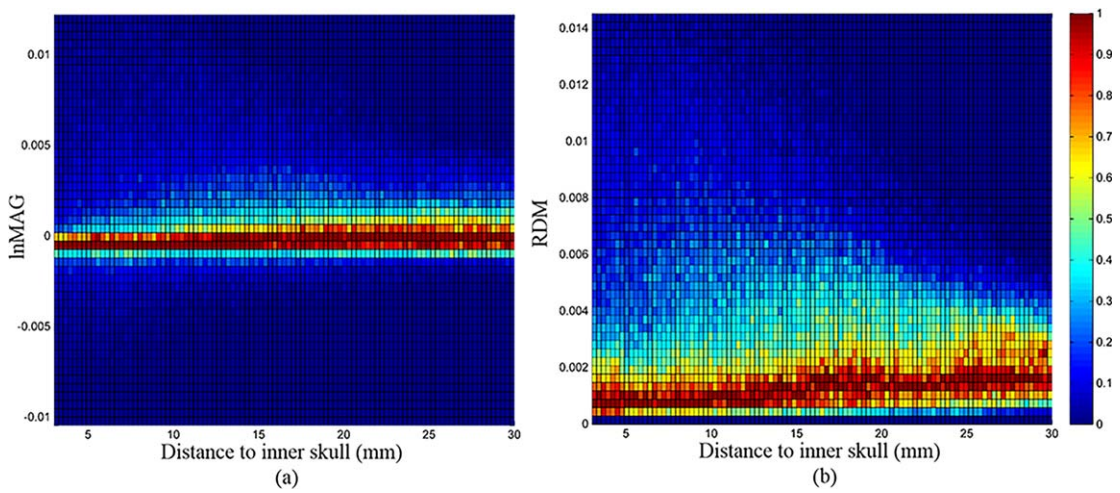

Figure 19.

Effect of fontanel conductivity. The 2D heat maps show differences in signal magnitude (lnMAG) and signal topography (RDM) between ModelT10 (white matter, gray matter, CSF, cranial bones (CB), fontanels, and scalp, $\sigma WM = 0.14$ S/m, $\sigma GM = 0.41$ S/m, $\sigma CSF = 1.79$ S/m, $\sigma CB = 0.04$ S/m, $\sigma fontanel = 0.54$ S/m, $\sigma scalp = 0.43$ S/m) and ModelR (white matter, gray matter, CSF, cranial bones, fontanels, and scalp, $\sigma WM = 0.14$ S/m, $\sigma GM = 0.33$ S/m, $\sigma CSF = 1.79$ S/m, $\sigma CB = 0.04$ S/m, $\sigma fontanel = 0.43$ S/m, $\sigma scalp = 0.43$ S/m). The difference between the two models is highlighted in bold. [Color figure can be viewed in the online issue, which is available at wileyonlinelibrary.com.]

Limitations and Future Work

Two issues in our study require further investigation. First, the influence of modeling WM anisotropy on adult EEG forward solutions and source analysis has already been investigated [Ramon et al., 2004; Vorwerk et al., 2014]. In neonates, WM is exposed to dramatic anisotropic changes in structure due to the maturation and myelination process. Its effect on forward modeling is, therefore, expected to increase. In this study, we did not investigate the effect of WM anisotropy because diffusion-tensor MRI scans are required to reconstruct anisotropic conductivity tensors and the three-dimensional architecture of WM tracts. Second, although we investigated the effects of various anatomical deficiencies and inaccuracies concerning head tissue conductivities on EEG forward modeling, it would be highly desirable to investigate the relationship between topographic and magnitude changes in forward modeling and the probable error in source localization, as in the study conducted in adults by Dannhauer et al. [2011].

CONCLUSION

We investigated the effect of uncertainty in conductivities of skull, fontanels, GM, and WM, and structural deficiencies including exclusion of CSF and fontanels and the discrimination between GM and WM on EEG forward solutions using a realistic neonatal head model. As a guide to EEG forward modelling, our study highlights key issues on how strongly EEG forward solutions are sensitive to imperfections in geometry and conductivity values of various head tissues in neonates. Our results emphasize the importance of CSF inclusion and GM/WM discrimination for EEG forward modeling due to their widespread intense effect. Uncertainty in GM and WM conductivity also caused widespread but less intense effects on EEG forward simulations. Exclusion of the fontanels induced weaker effects on the frontal, central, and temporal regions. Changes in the conductivity of the fontanels and the skull induced weak effects on EEG amplitudes limited to the cortical areas beneath the fontanels and the skull. These findings have practical implications for a better understanding of the importance of inaccuracies in conductivity and deficiencies in head tissue compartments and their impact on modeling research and localization of brain electrical activity in neonates.

REFERENCES

Adeyemo AA, Omotade OO (1999): Variation in fontanelle size with gestational age. Early Hum Dev 54:207–214.

Ahn S, Kim D, Hong JH, Jun SC (2012): Effect of realistic human head modelling on brain source distribution. Electron Lett 48: 1095–1097.

Akalin Acar Z, Makeig S (2013): Effects of Forward Model Errors on EEG Source Localization. Brain Topogr 26:378–396.

Beauchamp MS, Beurlot MR, Fava E, Nath AR, Parikh NA, Saad ZS, Bortfeld H, Oghalai JS (2011): The developmental trajectory of brain-scalp distance from birth through childhood: implications for functional neuroimaging. PloS one 6:e24981.

Dannhauer M, Lanfer B, Wolters CH, Knösche TR (2011): Modeling of the human skull in EEG source analysis. Hum Brain Mapp 32:1383–1399.

Despotovic I, Cherian PJ, De Vos M, Hallez H, Deburchgraeve W, Govaert P, Lequin M, Visser GH, Swarte RM, Vansteenkiste E, Van Huffel S, Philips W (2013): Relationship of EEG sources of neonatal seizures to acute perinatal brain lesions seen on MRI: A pilot study. Hum Brain Mapp 34:2402–2417.

Fang Q, Boas DA (2009): Tetrahedral mesh generation from volumetric binary and grayscale images. In: IEEE International Symposium on Biomedical Imaging: From Nano to Macro, 2009. ISBI '09. Boston, Massachusetts, USA, pp 1142–1145.

Gargiulo P, Belfiore P, Friðgeirsson EA, Vanhatalo S, Ramon C (2015): The effect of fontanel on scalp EEG potentials in the neonate. Clin Neurophysiol 126:1703–1710.

Ghadimi S, Abrishami-Moghaddam H, Kazemi K, Grebe R, Goundry-Jouet C, Wallois F, (2008): Segmentation of scalp and skull in neonatal MR images using probabilistic atlas and level set method. In: 30th Annual International Conference of the IEEE Engineering in Medicine and Biology Society, EMBS 2008. Vancouver, Canada, pp 3060–3063.

Güllmar D, Haueisen J, Reichenbach JR (2010): Influence of anisotropic electrical conductivity in white matter tissue on the EEG/MEG forward and inverse solution. A high-resolution whole head simulation study. NeuroImage 51:145–163.

Haueisen J, Ramon C, Brauer H, Nowak H (2000): The influence of local tissue conductivity changes on the Magnefoencephalogram and the Electroencephalogram - Der Einfluß der Änderung der lokalen Gewebeleitfähigkeit auf das Elektroenzephalogramm und das Magnetoenzephalogramm. Biomed Tech Eng 45:211–214.

Hughes JR (1996): A Review of the Usefulness of the Standard EEG in Psychiatry. Clin EEG Neurosci 27:35–39.

Kiesler J, Ricer R (2003): The abnormal fontanel. Am Fam Phys 67: 2547–2552.

Kwon MJ, Hahn J, Park H (2008): A fast spherical inflation method of the cerebral cortex by deformation of a simplex mesh on the polar coordinates. Int J Imaging Syst Technol 18:9–16.

Lanfer B, Scherg M, Dannhauer M, Knösche TR, Burger M, Wolters CH (2012): Influences of skull segmentation inaccuracies on EEG source analysis. NeuroImage 62:418–431.

Lew S, Wolters CH, Dierkes T, Röer C, MacLeod RS (2009): Accuracy and run-time comparison for different potential approaches and iterative solvers in finite element method based EEG source analysis. Appl Numer Math Trans IMACS 59:1970–1988.

Lew S, Sliva DD, Choe M, Grant PE, Okada Y, Wolters CH, Hämäläinen MS (2013): Effects of sutures and fontanels on MEG and EEG source analysis in a realistic infant head model. NeuroImage 76:282–293.

Li J, Wang K, Zhu S, He B (2007): Effects of holes on EEG forward solutions using a realistic geometry head model. J Neural Eng 4:197–204.

Mahmoudzadeh M, Dehaene-Lambertz G, Fournier M, Kongolo G, Goudjil S, Dubois J, Grebe R, Wallois F (2013): Syllabic discrimination in premature human infants prior to complete formation of cortical layers. Proceedings of the National Academy of Sciences of the United States of America 110: 4846–4851.

Marin G, Guerin C, Baillet S, Garnero L, Meunier G (1998): Influence of skull anisotropy for the forward and inverse problem

in EEG: Simulation studies using FEM on realistic head models. Hum Brain Mapp 6:250–269.

Meijs JWH, Weier OW, Peters MJ, van Oosterom A (1989): On the numerical accuracy of the boundary element method (EEG application). IEEE Trans Biomed Eng 36:1038–1049.

Montes-Restrepo V, van Mierlo P, Lopez JD, Hallez H, Vandenberghe S (2013): Influence of isotropic skull models on EEG source localization. Conference proceedings : ... Annual International Conference of the IEEE Engineering in Medicine and Biology Society. IEEE Engineering in Medicine and Biology Society. Annual Conference, 2013:3295–3298.

Mosher JC, Leahy RM, Lewis PS (1999): EEG and MEG: Forward solutions for inverse methods. IEEE Trans Biomed Eng 46:245–259.

Odabaee M, Tokariev A, Layeghy S, Mesbah M, Colditz PB, Ramon C, Vanhatalo S (2014): Neonatal EEG at scalp is focal and implies high skull conductivity in realistic neonatal head models. NeuroImage 96:73–80.

Pant S, Te T, Tucker A, Sadleir RJ (2011): The conductivity of neonatal piglet skulls. Physiological measurement 32:1275–1283.

Prastawa M, Gilmore JH, Lin W, Gerig G (2005): Automatic segmentation of MR images of the developing newborn brain. Med Image Anal 9:457–466.

Ramon C, Schimpf P, Haueisen J, Holmes M, Ishimaru A (2004): Role of soft bone, CSF and gray matter in EEG simulations. Brain Topogr 16:245–248.

Rampil IJ (1998): A Primer for EEG Signal Processing in Anesthesia. J Am Soc Anesthesiol 89:980–1002.

Rice JK, Rorden C, Little JS, Parra LC (2013): Subject position affects EEG magnitudes. NeuroImage 64:476–484.

Roche-Labarbe N, Aarabi A, Kongolo G, Gondry-Jouet C, Dümpelmann M, Grebe R, Wallois F (2008): High-resolution electroencephalography and source localization in neonates. Hum Brain Mapp 29:167–176.

Rorden C, Bonilha L, Fridriksson J, Bender B, Karnath HO (2012): Age-specific CT and MRI templates for spatial normalization. NeuroImage 61:957–965.

Sadler TW, Langman J (2000): Langman's Medical Embryology. Philadelphia: Lippincott Williams & Wilkins.

Salinsky M, Kanter R, Dasheiff RM (1987): Effectiveness of multiple EEGs in supporting the diagnosis of epilepsy: An operational curve. Epilepsia 28:331–334.

Vallaghe S, Clerc M (2009): A global sensitivity analysis of three- and four-layer EEG conductivity models. IEEE Trans Biomed Eng 56:988–995.

Vorwerk J, Cho JH, Rampp S, Hamer H, Knösche TR, Wolters CH (2014): A guideline for head volume conductor modeling in EEG and MEG. NeuroImage 100:590–607.

Wallois F, Mahmoudzadeh M, Patil A, Grebe R (2012): Usefulness of simultaneous EEG–NIRS recording in language studies. Brain Lang 121:110–123.

Wieser HG, Schindler K, Zumsteg D (2006): EEG in Creutzfeldt–Jakob disease. Clin Neurophysiol 117:935–951.

Wolters CH, Köstler H, Möller C, Härdtlein J, Anwander A (2007): Numerical approaches for dipole modeling in finite element method based source analysis. Int Congr Ser (New Frontiers in Biomagnetism. Proceedings of the 15th International Conference on Biomagnetism, Vancouver, BC, Canada, August 21–25, 2006) 1300:189–192.